Enhanced low-rank plus group sparse decomposition for speckle reduction in OCT images

Kopriva, Ivica, Shi, Fei, Štanfel, Marija, Chen, Xinjian

Ivica Kopriva, Fei Shi, Marija Štanfel, Xinjian Chen, "Enhanced low-rank plus group sparse decomposition for speckle reduction in OCT images," Proc. SPIE 11313, Medical Imaging 2020: Image Processing, 113132H (10 March 2020); doi: 10.1117/12.2538466

SPIE.

Event: SPIE Medical Imaging, 2020, Houston, Texas, United States

Enhanced low-rank plus group sparse decomposition for speckle reduction in OCT images

Ivica Kopriva[1*], Fei Shi[3,] Marija Štanfel[2], and Xinjian Chen[3,4]

[1]Division of Electronics, Ruđer Bošković Institute, Bijenička cesta 54, P.O. Box 180, 10002, Zagreb, Croatia
[2]Department of Ophthalmology, University Hospital Center Zagreb, Kišpatićeva 12, Zagreb 10000, Croatia
[3]School of Electronics and Information Engineering, Soochow University, No. 1 Shizi Street, Suzhou, 215006, China
[4]State Key Laboratory of Radiation Medicine and Protection, Soochow University, 199 Renai Road, Suzhou, 215123, China

e-mail: ikopriva@irb.hr, stanfel.m@gmail.com, shifei@suda.edu.cn, xjchen@suda.edu.cn

Abstract

Suppression of speckle artifact in optical coherence tomography (OCT) is necessary for high quality quantitative assessment of ocular disorders associated with vision loss. However, due to its dual role as a source of noise and as a carrier of information about tissue microstructure, complete suppression of speckle is not desirable. That is what represents challenge in development of methods for speckle suppression. We propose method for additive decomposition of a matrix into low-rank and group sparsity constrained terms. Group sparsity constraint represents novelty in relation to state-of-the-art in low-rank sparse additive matrix decompositions. Group sparsity enforces more noise-related speckle to be absorbed by the sparse term of decomposition. Thus, the low-rank term is expected to enhance the OCT image further. In particular, proposed method uses the elastic net regularizer to induce the grouping effect. Its proximity operator is shrunken version of the soft-thresholding operator. Thus, the group sparsity regularization adds no extra computational complexity in comparison with the ℓ_1 norm regularized problem. We derive alternating direction method of multipliers based algorithm for related optimization problem. New method for speckle suppression is automatic and computationally efficient. The method is validated in comparison with state-of-the-art on ten 3D macular-centered OCT images of normal eyes. It yields OCT image with improved contrast-to-noise ratio, signal-to-noise ratio, contrast and edge fidelity (sharpness).

Keywords: Optical coherence tomography, speckle, additive image decomposition, low-rankness, group sparsity.

Medical Imaging 2020: Image Processing, edited by Ivana Išgum, Bennett A. Landman,
Proc. of SPIE Vol. 11313, 113132H · © 2020 SPIE · CCC
code: 1605-7422/20/$21 · doi: 10.1117/12.2538466

1 INTRODUCTION

Speckle is inherent random signal modulation caused by spatial and temporal coherence of the optical waves. The coherence represents basis for interferometry, the measurement technique upon which optical coherence tomography (OCT) is founded [1-3]. Thus, speckle has dual role as a source of noise and as a carrier of information about tissue microstructure [2]. Therefore, complete speckle reduction is not desirable. However, in OCT images of biological specimens speckle reduce contrast and make boundaries between constitutive tissues more difficult to resolve [1, 2, 4]. That, in return, stands for major obstacle in quantitative OCT image analysis, [1, 5, 2], what is necessary to discriminate pathological states of tissue, [6, 7], such as cystoid macular edema [8], central retinal artery occlusion [9], atherosclerosis plaques [10], etc. Speckle reduction techniques belong to two groups: physical compounding and digital filtering [1]. The physical compounding strategies achieve OCT image quality improvement proportional to the square root of the number of realizations. Digital filtering methods aim to reduce speckle through post-processing of OCT image, while preserving image resolution, contrast and edge fidelity [11-13]. However, as it is demonstrated in [14], state-of-the-art digital filtering methods such as median filtering, can even decrease sharpness when reducing speckle. Therefore, conceptually new low-rank and sparsity decomposition method, named enhanced low-rank plus sparsity decomposition (ELpSD) algorithm, was proposed in [14] to reduce speckle in OCT images. The method proposed herein stands for new contribution in additive matrix decomposition into sum of low-rank and sparse matrices. The novelty is related to hybrid regularization for sparseness in order to achieve the grouping effect. The group sparsity constraint, as opposed to sparsity constraint only, is relevant in feature selection via sparse regression when features within some group are correlated [15, 16]. Sparsity constraint alone picks up only the most dominant variable within the group. The fact that speckle belong to two groups, the one provided information on tissue microstructure and the one related to noise, motivated us to develop group sparsity constrained method for speckle reduction. That is expected to further enforce noise-related speckle to be absorbed in sparsity term of additive OCT image decomposition. That, in turn, is expected to further improve quality of enhanced OCT image. Let us denote logarithm of the intensity of one 2D OCT image as **X**. Exact decomposition **X**=**L**+**S**, where **L** stands for the low-rank and **S** for sparse matrix, has been known under the name robust principal component analysis (RPCA) [17] or rank-sparsity decomposition [18]. As properly noted in [19], adding the "noise" term **G** to the RPCA model, that is **X**=**L**+**S**+**G**, describes empirical data more realistically. However, the fundamental issue in low-rank and sparse decomposition is accuracy of approximation of rank and sparseness. Both functions are discrete and non-convex and stand for, respectively, number of nonzero singular values of **L** and number of nonzero coefficients of **S**. To avoid difficulties associated with discrete non-polynomial (NP)-hard optimization, rank and sparseness minimization problems are often replaced by convex relaxation [17, 20-23]. In case of rank that is known as nuclear- or Schatten-1 norm, [24, 25], and it stands for ℓ_1-norm of the vector of singular values. In case of sparseness, convex relaxation refers to ℓ_1-norm of a corresponding matrix. Several recent studies have emphasized the benefit of nonconvex penalty functions compared to the nuclear norm for the estimation of the singular values [26, 20, 27, 28]. In particular, it has been presented in [26] how nonconvex regularization, that promotes sparser approximation of singular values [29], can be combined into convex optimization problem related to the estimation of the low-rank matrices. This regularization has been used in [14] to develop the

ELRpSD speckle reduction method. However, to further reduce influence of the speckle noise we propose to introduce the group sparsity regularization for **S** in the presence of additive white Gaussian noise (AWGN) **G**, i.e. **X=L+S+G**. In particular, in comparison with the ELRpSD method [14], that uses non-convex regularizer for a rank of **L** and ℓ_1-norm regularizer for sparseness of **S**, proposed method uses hybrid ℓ_{1+2}-norm regularizer for (group) sparsity of **S**. The ℓ_{1+2}-norm regularizer, a.k.a. the elastic net regularizer [30], induces the grouping effect. Nonetheless, it is also important that its proximity operator is actually shrunken version of the soft-thresholding operator (it represents the proximity operator of the ℓ_1 norm) [31]. Thus, the group sparsity regularization adds no extra computational complexity in comparison with the ELRpSD method. It actually increases speed of convergence. We name the proposed method enhanced low-rank plus group sparsity decomposition (ELRpGSD). As it is demonstrated in Sec. 3, it yields OCT image with simultaneously improved contrast-to-noise ratio (CNR), signal-to-noise ratio (SNR), contrast and edge fidelity (sharpness). In particular, depending on the value of the constant related to the additional ℓ_2 regularization term, CNR and contrast can be improved significantly in comparison with the ELRpSD method while SNR and sharpness are decreased mildly. Thus, depending on the relative importance of the each image quality metric the group sparsity regularization can bring additional improvement of the quality of OCT images. Because they use the same regularization for rank, the ELRpGSD method analogously to the ELRpSD method does not require *a priori* information of the rank value. That in combination with the group sparsity regularization represents the main distinctions with respect to the RPCA based methods for OCT image enhancement [32, 33]. The ELRpGSD method is illustrated in Figs. 1(a) to 1(c). For the sake of visual comparison we present, in respective order, in Fig. 1(d) to Fig. 1(g) results of OCT image enhancement by ELRpSD algorithm [14], by the GoDec algorithm [17] as well as by 2D bilateral and median filtering (see Sec. 3 for more details). The rest of this paper is organized as follows. The details of the proposed ELRpSGD method are presented in Sec. 2. That is followed by an experimental comparative performance analysis in Sec. 3 and the discussion in Sec. 4. The conclusions are presented in Sec. 5.

2 MATERIALS AND METHODS

Let $\mathbf{X} \in \mathbb{R}_{0+}^{I_1 \times I_2}$ be one scan of the 3D OCT image with the size of $I_1 \times I_2$ pixels. The speckle, which occurs due to the random scattering of the light on tissues, acts effectively as multiplicative noise [1]. That is, $x(i_1,i_2) = l(i_1,i_2) \times s(i_1,i_2)$, where (i_1,i_2) stands for pixel coordinates and $x(i_1,i_2)$ stands for the intensity value at (i_1,i_2). By taking the log of $x(i_1,i_2)$ we obtain:

$$\log x(i_1,i_2) = \log l(i_1,i_2) + \log s(i_1,i_2) \tag{1}$$

With the slight abuse of notation we rewrite (1) on the matrix level as:

$$\mathbf{X} = \mathbf{L} + \mathbf{S} + \mathbf{G} \tag{2}$$

where, in relation to Eq.(1), the AWGN term **G** with zero mean and unknown variance σ^2 has been added. We provide the same justification of the model (2) as in [14]. Due to the random nature of the scattering, the speckle associated with the matrix **S** has sparse spatial distribution. Thus, the matrix **L** represents enhanced OCT image that contains information on tissue microstructure. Hence, it is justified to assume that **L** is low-rank approximation of **X** [32, 33]. Thus, reduction of the speckle within the OCT image can be seen as decomposition of the empirical data matrix (OCT image) **X** into low-rank matrix **L** and sparse matrix **S**. Herein, by introducing the group sparsity constraint we want the noise related speckle to be absorbed even more in the sparse matrix **S**.

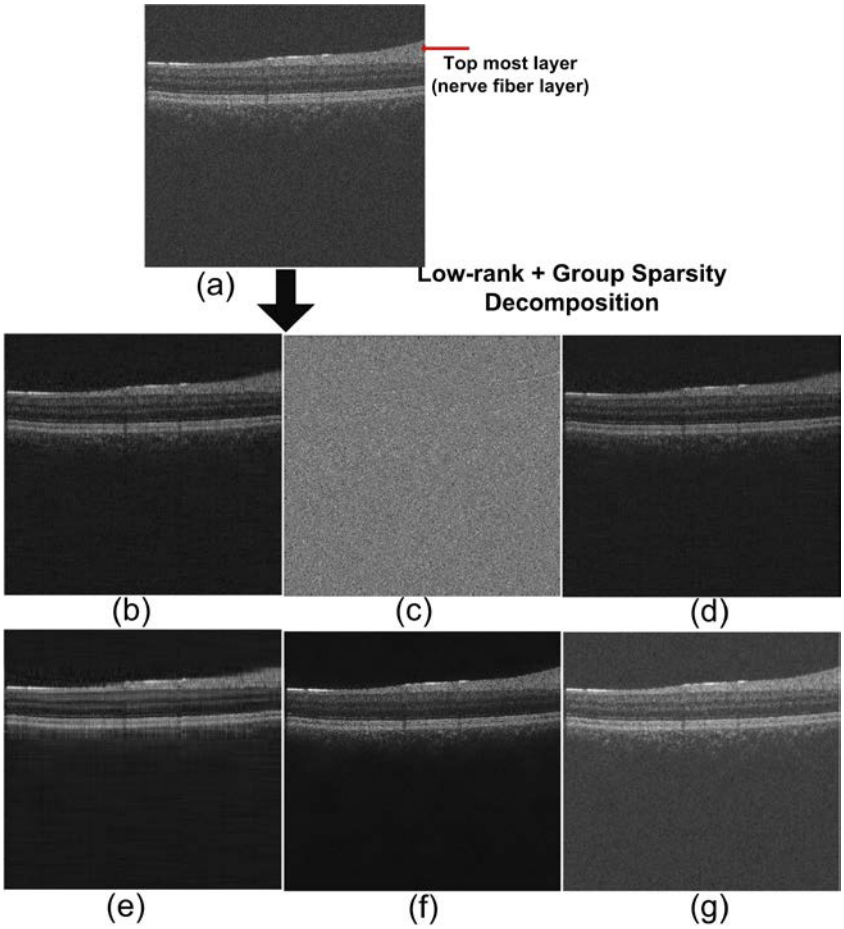

Figure 1. (a) to (c): flow chart of the "low-rank + group sparsity" decomposition approach to speckle reduction in optical coherence tomography (OCT) images. Information on image quality metrics such as contrast-to-noise ratio (CNR), signal-to-noise ratio (SNR) in dB, contrast and sharpness, can be found in Sec. 2.2. (a) original OCT image: CNR = 3.61, SNR = 12.51, contrast = 1.14, sharpness = 56.90. (b) ELRpGSD-based approximation of OCT image: CNR=4.22, SNR=13.71, contrast=1.47, sharpness=61.49. (c) Sparse term containing speckle. (d) ELRpSD-based approximation of OCT image: CNR = 4.18, SNR = 13.85, contrast = 1.45, sharpness = 61.06. (e) OCT image enhanced by the GoDec algorithm (rank=35):[19] CNR = 4.59, SNR = 6.43, contrast = 1.71, sharpness = 49.01. (f) OCT image enhanced by bilateral filtering: CNR = 4.19, SNR = 10.58, contrast = 1.65, sharpness = 59.79. (g) OCT image enhanced by median filtering: CNR = 9.09, SNR = 6.08, contrast = 1.97, sharpness = 37.79. For visual comparison OCT images (a) to (g) were mapped to [0 1] interval with the MATLAB mat2gray command from the interval corresponding to minimal and maximal values of each specific case. The best value for each figure of merit is in bold.

2.1 Enhanced low-rank and group sparsity regularized additive decomposition

Estimation of the low-rank matrix **L** and sparse matrix **S** is expressed as the following optimization problem:

$$\min_{\mathbf{L},\mathbf{S}} \ \lambda\, rank(\mathbf{L}) + \tau \left\|\mathbf{S}\right\|_0 \quad subject\ to \quad \mathbf{X} = \mathbf{L} + \mathbf{S} + \mathbf{G} \tag{3}$$

Here, $\left\|\mathbf{S}\right\|_0$ stands for ℓ_0 pseudo-norm that counts the number of nonzero entries of **S** while λ and τ are nonnegative tuning parameters. Rank minimization problem is NP-hard. Minimization of the number of nonzero entries is NP-hard problem as well. Thus, optimization problem (3) is often replaced by convex relaxation [17, 20]:

$$\min_{\mathbf{L},\mathbf{S}} \ \lambda \sum_i \sigma_i(\mathbf{L}) + \tau \left\|\mathbf{S}\right\|_1 \quad subject\ to \quad \mathbf{X} = \mathbf{L} + \mathbf{S} + \mathbf{G} \tag{4}$$

The first term is the ℓ_1-norm of the vector $\boldsymbol{\sigma}(\mathbf{L}) \in \mathbb{R}_{0+}^{\min(I_1, I_2)}$ of singular values of **L**, and it is known as the nuclear- or Schatten-1 norm of **L** [24, 25]. It represents convex relaxation of the rank minimization problem [21]. The second term is the ℓ_1-norm of the matrix **S** and it represents convex relaxation of the $\left\|\mathbf{S}\right\|_0$ minimization problem [34]. Because nuclear norm is not accurate measure of rank non-convex regularization that promotes more sparse approximation of singular values was used for rank approximation in [14] converting (4) into the following optimization problem:

$$\min_{\mathbf{L},\mathbf{S}} \left\{ \Psi(\mathbf{L},\mathbf{S}) = \frac{1}{2}\left\|\mathbf{X} - \mathbf{L} - \mathbf{S}\right\|_F^2 + \lambda \sum_{i=1}^{k} \phi\left(\sigma_i(\mathbf{L}); a\right) + \tau \left\|\mathbf{S}\right\|_1 \right\} \tag{5}$$

where function ϕ is the partly quadratic penalty function such that for parameter $0 \le a < 1/\lambda$ the resulting low-rank optimization subproblem of (5) is convex [26]. In order to collect the noise related speckle more efficiently we additionally introduce ℓ_2-norm regularization for **S**:

$$\min_{\mathbf{L},\mathbf{S}} \left\{ \Psi(\mathbf{L},\mathbf{S}) = \frac{1}{2}\left\|\mathbf{X} - \mathbf{L} - \mathbf{S}\right\|_F^2 + \lambda \sum_{i=1}^{k} \phi\left(\sigma_i(\mathbf{L}); a\right) + \tau \left\|\mathbf{S}\right\|_1 + \gamma \left\|\mathbf{S}\right\|_2 \right\} \tag{6}$$

This type of regularization is in sparse regression known as elastic net and it is used for grouping features that belong to the same category [30]. Optimization problem (6) can be split into two sub-

problems: the rank minimization problem when **S** is fixed and the group sparsity minimization problem when **L** is fixed. Thus, we need to find proximity operators of $\phi\left(\sigma_i(\mathbf{L});a\right)$ and of $\tau\|\mathbf{S}\|_1+\gamma\|\mathbf{S}\|_2$. The proximity operator of $\phi\left(\sigma_i(\mathbf{L});a\right)$ $\theta:\mathbb{R}\to\mathbb{R}$ defined as:

$$\theta\left(y;\lambda,a\right):=\arg\min_{x\in\mathbb{R}}\left\{\frac{1}{2}\left(y-x\right)^2+\lambda\phi\left(x;a\right)\right\} \tag{7}$$

was shown to be the firm threshold function [26]:

$$\theta\left(y;\lambda,a\right):=\min\left\{|y|,\max\left(\left(|y|-\lambda\right)/\left(1-a\lambda\right),0\right)\right\}sign\left(y\right) \tag{8}$$

In case of matrix **X**, notation $\theta\left(\mathbf{X};\lambda,a\right)$ implies that the proximal operator is applied element-wise to **X**. Proximity operator of the sparsity related term in (6) amounts to computing proximity operator of the sum of regularizing functions. Let us denote:

$$g\left(\mathbf{S}\right)=\|\mathbf{S}\|_1,\ h\left(\mathbf{S}\right)=\|\mathbf{S}\|_2 \tag{9}$$

Let us define the proximity operator $P_g(\mathbf{Y})$:

$$P_g\left(\mathbf{Y}\right):=\arg\min_{\mathbf{X}\in\mathbb{R}^{I_1\times I_2}}\left\{\frac{1}{2}\left(\mathbf{X}-\mathbf{Y}\right)^2+\tau g\left(\mathbf{X}\right)\right\} \tag{10}$$

$P_g(\mathbf{Y})$ admits analytical solution in a form of the soft thresholding function [35]:

$$P_g\left(\mathbf{Y}\right)=S_\tau\left(\mathbf{Y}\right)=\max\left(|\mathbf{Y}|-\tau,0\right)sign\left(\mathbf{Y}\right) \tag{11}$$

such that the soft threshodling operation is applied on **Y** entry wise. In general the proximity operator $P_{g+h}\left(\mathbf{Y}\right)$ does not have analytical solution, i.e. $P_{g+h}\left(\mathbf{Y}\right)\neq P_g\left(\mathbf{Y}\right)+P_h\left(\mathbf{Y}\right)$ [31, 36]. However, for $g(\mathbf{S})$ and $h(\mathbf{S})$ given by (9) it is shown that [31]:

$$P_{g+\gamma h}\left(\mathbf{Y}\right)=S_{\tau/(1+\gamma)}\left(\mathbf{Y}\right) \tag{12}$$

In other words, an extra ℓ_2 regularizer tends to double "shrink" the solution [31]. Thus, the optimization problem (6) can be replaced by an equivalent optimization problem:

$$\min_{\mathbf{L},\mathbf{S}} \left\{ \Psi(\mathbf{L},\mathbf{S}) = \frac{1}{2}\left\|\mathbf{X}-\mathbf{L}-\mathbf{S}\right\|_F^2 + \lambda\sum_{i=1}^{k}\phi\left(\sigma_i(\mathbf{L});a\right) + \frac{\tau}{1+\gamma}\left\|\mathbf{S}\right\|_1 \right\} \tag{13}$$

We derive algorithm for optimization problem (13) using alternating direction method of multipliers (ADMM) [37]. Thus, we formulate the augmented Lagrangian [38] for problem (13):

$$L(\mathbf{L},\mathbf{S},\mathbf{\Lambda}) = \lambda\sum_{i=1}^{k}\phi\left(\sigma_i(\mathbf{L});a\right) + \frac{\tau}{1+\gamma}\left\|\mathbf{S}\right\|_1 + \left\langle\mathbf{\Lambda},\mathbf{X}-\mathbf{L}-\mathbf{S}\right\rangle + \frac{\mu}{2}\left\|\mathbf{X}-\mathbf{L}-\mathbf{S}\right\|_F^2 \tag{14}$$

The rank minimization problem, when **S** is fixed, yields:

$$\begin{aligned}
\mathbf{L}_t &= \arg\min_{\mathbf{L}} L\left(\mathbf{L},\mathbf{S}_{t-1},\mathbf{\Lambda}_{t-1},\mu_{t-1}\right) \\
&= \arg\min_{\mathbf{L}}\ \lambda\sum_{i=1}^{k}\phi\left(\sigma_i(\mathbf{L});a\right) + \left\langle\mathbf{\Lambda},\mathbf{X}-\mathbf{L}-\mathbf{S}_{t-1}\right\rangle + \frac{\mu_{t-1}}{2}\left\|\mathbf{X}-\mathbf{S}_{t-1}-\mathbf{L}\right\|_F^2 \\
&= \arg\min_{\mathbf{L}}\ \lambda\sum_{i=1}^{k}\phi\left(\sigma_i(\mathbf{L});a\right) + \frac{\mu_{t-1}}{2}\left\|\mathbf{X}-\mathbf{S}_{t-1}-\mathbf{L}+\frac{\mathbf{\Lambda}_{t-1}}{\mu_{t-1}}\right\|_F^2
\end{aligned} \tag{15}$$

where *t* denotes iteration index. Let $\mathbf{U\Sigma V}^{\mathrm{T}}$ denotes singular value decomposition (SVD) of:

$$\mathbf{U\Sigma V}^T = SVD\left(\mathbf{X}-\mathbf{S}_{t-1}+\frac{\mathbf{\Lambda}_{t-1}}{\mu_{t-1}}\right) \tag{16}$$

Applying (7) and (8) to (15) yields solution for low-rank matrix **L** at iteration *t*:

$$\mathbf{L}_t = \mathbf{U}\theta\left(\mathbf{\Sigma};\lambda/\mu_{t-1},a\right)\mathbf{V}^T \tag{17}$$

Sparseness minimization problem, when **L** is fixed, yields:

$$\begin{aligned}
\mathbf{S}_t &= \arg\min_{\mathbf{S}} L\left(\mathbf{L}_t,\mathbf{S},\mathbf{\Lambda}_{t-1},\mu_{t-1}\right) \\
&= \arg\min_{\mathbf{S}}\ \frac{\tau}{1+\gamma}\left\|\mathbf{S}\right\|_1 + \left\langle\mathbf{\Lambda},\mathbf{X}-\mathbf{L}_t-\mathbf{S}\right\rangle + \frac{\mu_{t-1}}{2}\left\|\mathbf{X}-\mathbf{L}_t-\mathbf{S}\right\|_F^2 \\
&= \arg\min_{\mathbf{S}}\ \frac{\tau}{1+\gamma}\left\|\mathbf{S}\right\|_1 + \frac{\mu_{t-1}}{2}\left\|\mathbf{X}-\mathbf{L}_t-\mathbf{S}+\frac{\mathbf{\Lambda}_{t-1}}{\mu_{t-1}}\right\|_F^2
\end{aligned} \tag{18}$$

Applying (10) and (11) to (18) yields solution for sparse matrix **S** at iteration *t*:

$$\mathbf{S}_t = S_{\frac{\tau}{(1+\gamma)\mu_{t-1}}}\left(\mathbf{X}-\mathbf{L}_t+\frac{\mathbf{\Lambda}_{t-1}}{\mu_{t-1}}\right) \tag{19}$$

Matrix of Lagrange multipliers at iteration *t* is updated according to:

$$\mathbf{\Lambda}_t = \mathbf{\Lambda}_{t-1}+\mu_{t-1}\left(\mathbf{X}-\mathbf{L}_t-\mathbf{S}_t\right) \tag{20}$$

and penalization parameter is updated according to:

$$\mu_t = \max\left\{\rho\mu_{t-1}, \mu^{\max}\right\} \tag{21}$$

where ρ stands for adaptation rate and $\mu^{\max}$ is the maximal value of the penalization parameter. In our experiments, however, we found out that algorithms converges for μ_t=1. The algorithm is stopped when either predefined number of iterations is reached or when root mean square error (RMSE) is bellow some predefined threshold ε:

$$\left\|\mathbf{X}-\mathbf{L}_t-\mathbf{S}_t\right\|_2 \le \varepsilon \tag{22}$$

We demonstrate numerically convergence of proposed ELRpGSD algorithm in Fig. 2. The ELRpSGD algorithm is summarized in Algorithm 1.

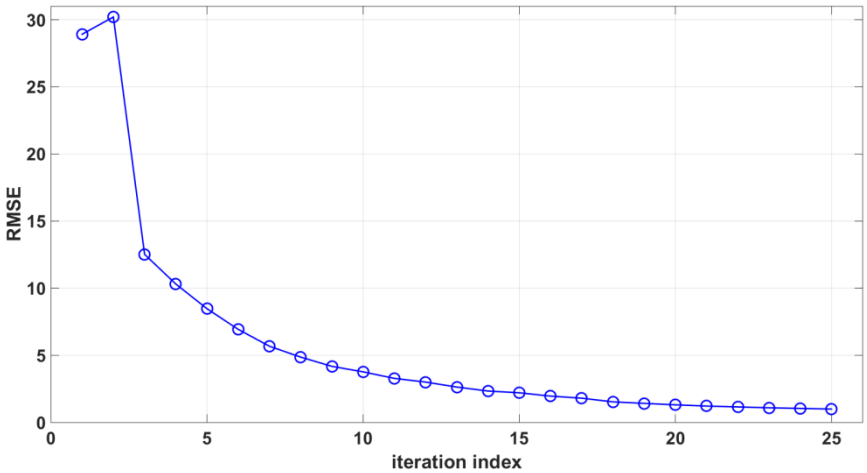

Figure 2. Convergence in term of the RMSE (22) as a function of the iteration index of the ELRpGSD algorithm for γ=0.4, τ=0.1, λ=5 and μ=1.

Algorithm 1. The ELRpGSD algorithm.

Input: logarithm of acquired OCT image $\mathbf{X} \in \mathbb{R}^{I_1 \times I_2}$ with the size of $I_1 \times I_2$ pixels, regularization constants λ, τ and γ related respectively to enhanced low-rank OCT image L and speckle term S in (13)/(14), RMSE threshold ε in (22). Suggested values: λ=5, τ=0.1, γ=0.4. Suggested value for the adaptive penalty parameter μ in (8)-(15): μ=1. Suggested value for stopping criterion in (22): ε=0.1.

1. $\mathbf{L}_{(0)} = \mathbf{0}$; $\mathbf{S}_{(0)} = \mathbf{0}$; $\mathbf{\Lambda}_{(0)} = 0$; t=1.
2. *while* not converged *do*
3. Execute SVD (16).
4. Update **L** using (17).
5. Update **S** using (19).
6. Update $\mathbf{\Lambda}$ using (20).
7. $t \leftarrow t+1$
8. *end while*

Output: $\mathbf{L} \leftarrow \mathbf{L}_{(t+1)}$, $\mathbf{S} \leftarrow \mathbf{S}_{(t+1)}$.

3 EXPERIMENTS AND RESULTS

3.1 Performance measure

To quantify the performance of speckle reduction algorithms, appropriate measures have to be defined. We use the same no-reference OCT image quality metrics as in [14]. In order to have the current paper self-contained we repeat their description as in Sec. 2.3 in [14]. In the case of OCT image, the most commonly used figure of merit is CNR [1, 2]. It corresponds to the inverse of the speckle fluctuation and it is defined as: $CNR = \mu_l(\mathbf{X}) / \sigma_l(\mathbf{X})$ where $\mu_l(\mathbf{X})$ and $\sigma_l(\mathbf{X})$ respectively correspond to the mean and standard deviation in some selected homogeneous part of the image **X**. Experimental results reported in Sec. 3 were estimated in the region that corresponds with the top most layer in the OCT image of a retina, which is indicated in Figure1 by red arrow [9]. Since the goal of post-processing algorithms is not only to reduce speckle but also to preserve image resolution, contrast and edge fidelity [1], we also estimate contrast, sharpness as well as SNR measures directly from the image. Sharpness is the attribute related to the preservation of fine details (edges) in an image. Contrast is defined as the ratio of the maximum and the minimum intensity of the entire image [39]. It reflects the strength of the noise or modeling error term **G**. Up to some extent it can be considered as an image quality measure that coincides with the SNR quality measure. Technical details on estimation of sharpness and contrast can be found in the [39, 14]. We estimated sharpness in the entire retinal region from the first (top most) to the tenth (bottom most) layer. Contrast was estimated from the whole image. By following [13], global SNR value was estimated as $SNR = 10\log\left[\max\left(\mathbf{X}_{lin}\right)^2 \Big/ \sigma_{lin}^2\right]$, where $\mathbf{X}_{lin}$ is the OCT image on a linear intensity scale and σ_{lin}^2, such that the noise variance was estimated on a region between top of the image and the top most layer.

3.2 Algorithms for comparison and OCT image acquisition

We compare the proposed ELRpGSD algorithm with: the ELRpSD algorithm [14], the 2D bilateral filtering algorithm and 2D median filtering algorithm. It has been shown in [14] that ELRpSD algorithm yields comparable or better performance than other algorithms that are based on additive low-rank and sparse decompositions such as GoDec [19] and SSGoDec [19] and the rank N soft constraint (RNSC) for RPCA algorithm [40]. The advantage of the ELRpGSD and the ELRpSD algorithms in comparison with GoDec, SSGoDec and RNSC algorithms is that later group demands *a priori* information on the rank and that requires tuning. That is why ELRpSD algorithm was selected to represent additive decomposition based OCT image enhancement methods. The MATLAB code for the 2D bilateral filtering algorithm has been downloaded from [41]. For 2D median filtering the MATLAB function median2 has been used. The speckle reduction algorithms were comparatively tested on 10 3D macular-centered OCT images of normal eyes acquired with the Topcon 3D OCT-1000 scanner. Each 3D OCT image was comprised of 64 2D scans with the size of 480×512 pixels. These images have been used previously for the study for optical intensity analysis in [42], where they were segmented into 10 retina layers. We estimated CNR-, SNR-, contrast- and sharpness values from the original image as well as from the images with reduced speckle. The images were analyzed with software written in the MATLAB® (the MathWorks Inc., Natick, MA) script language on PC with Intel i7 CPU with the clock speed of 2.2 GHz and 16GB of RAM.

3.3 Comparative results

We present the results of the comparative performance analysis between the ELRpGSD, ELRpSD, 2D bilateral filtering and 2D median filtering algorithms. Parameters of bilateral filter have been tuned to yield approximately the same CNR value (the same level of speckle reduction) as the ELRpSD algorithm [14]. The median filtering has been used with the window of the size 3×3 pixels. The algorithms were applied to each 2D OCT scan separately. CNR, SNR, contrast and sharpness were estimated from each enhanced 2D scan and the reported values were averaged over 64 scans for each 3D OCT image. Afterwards, they were averaged further over 10 3D OCT images. Average computation time of the ELRpGSD, ELRpSD, 2D bilateral filtering and 2D median filtering algorithms is per one 2D OCT scan respectively given as: 6.05s, 9.79s, 18.98s and 0.05s. Means and standard deviations averaged over 10 3D OCT images are presented in Table 1 for relative values of CNR, sharpness, contrast and SNR. Means and standard deviations of relative values are defined as in [14]. We provide information for relative SNR value as an example:

$$\text{Relative\_mean\_SNR}[\%] = 100 * \frac{\text{mean(SNR\_of\_enhanced image)-mean(SNR\_of\_original\_image)}}{\text{mean(SNR\_of\_original\_image)}} \tag{23}$$

$$\text{Relative\_standard\_deviation\_SNR}[\%] = 100 * \frac{\text{std(SNR\_of\_enhanced image-SNR\_of\_original\_image)}}{\text{mean(SNR\_of\_original\_image)}} \quad (24)$$

Relative values of CNR, contrast and sharpness were defined analogously. As can be seen from Table 1, ELRpGSD method is capable to further improve CNR value comparable with the ELRpSD method. In addition to that it also improves contrast with the mild decrease of sharpness and SNR. Bilateral and median filtering decrease SNR relative to the original OCT images, while median filtering also has negative relative value of sharpness. Thus, we further compare the ELRpGSD and ELRpSD algorithms in Figs. 3 to 6. Please note that the ELRpSD method follows as a special case of the ELRpGSD method when ℓ_2-norm regularization term is set γ=0, see Eq.(6) and 813). Figs. 3 to 6 show in respective order averaged values of absolute CNR, relative contrast, relative sharpness and relative SNR estimated from 10 3D OCT images. It can be seen that by increase of the regularization constant γ, CNR and contrast values are increased, while sharpness and SNR values are mildly decreased. Hence, depending on the relative importance of the each image quality metric the group sparsity regularization can bring additional improvement of the quality of OCT images. Fig. 7 shows relative values of all four metrics for each of 10 3D OCT images enhanced by the ELRpGSD algorithm with γ=0.4.

Table 1. Means and standard deviations of relative values of CNR, sharpness, contrast and SNR, (in percentage) averaged over 10 3D OCT images.

	CNR	**Sharpness**	**Contrast**	**SNR**
ELRpGSD, γ=0.4	13.39 ± 4.16	14.30 ± 2.70	27.02 ± 1.71	5.67 ± 6.80
ELRpGSD, γ=0.8	13.95 ± 4.36	13.68 ± 2.78	27.77 ± 13.68	5.26 ± 6.71
ELRpSD	12.02 ± 3.80	14.62 ± 2.5	24.54 ± 1.56	6.49 ± 6.90
Bilateral filtering	13.15 ± 3.50	4.42 ± 6.89	41.71 ± 3.19	-10.18 ± 2.38
Median filtering	151.9 ± 21.98	-30.35 ± 2.64	71.58 ± 2.23	-59.95 ± 9.19

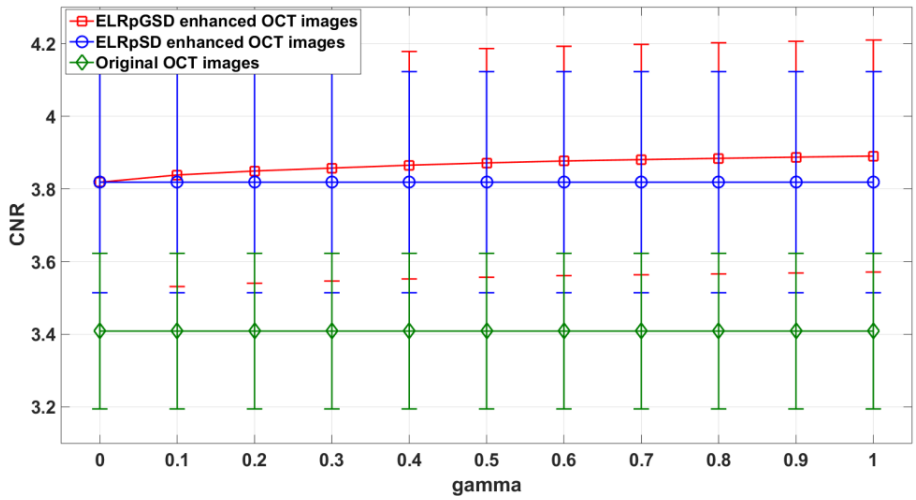

Figure 3. Average of absolute CNR values estimated from 10 3D OCT images: diamonds - original images; circles - images enhanced with the ELRpSD method; squares - images enhanced with the ELRpGSD method as a function of regularization constant γ, see Eq.(6) and (13).

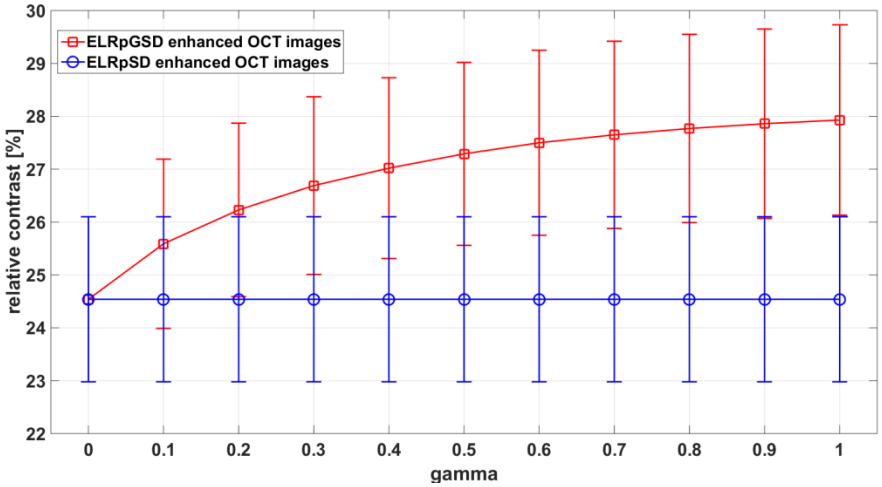

Figure 4. Average of relative contrast values (in percentage) estimated from 10 3D OCT images enhanced with: circles - the ELRpSD method; squares - the ELRpGSD method as a function of regularization constant γ, see Eq.(6) and (13).

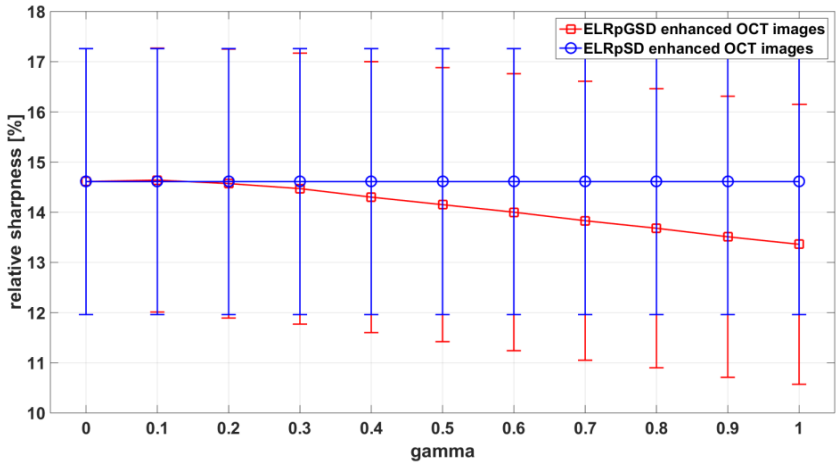

Figure 5. Average of relative sharpness values (in percentage) estimated from 10 3D OCT images enhanced with: circles - the ELRpSD method; squares - the ELRpGSD method as a function of regularization constant γ, see Eq.(6) and (13).

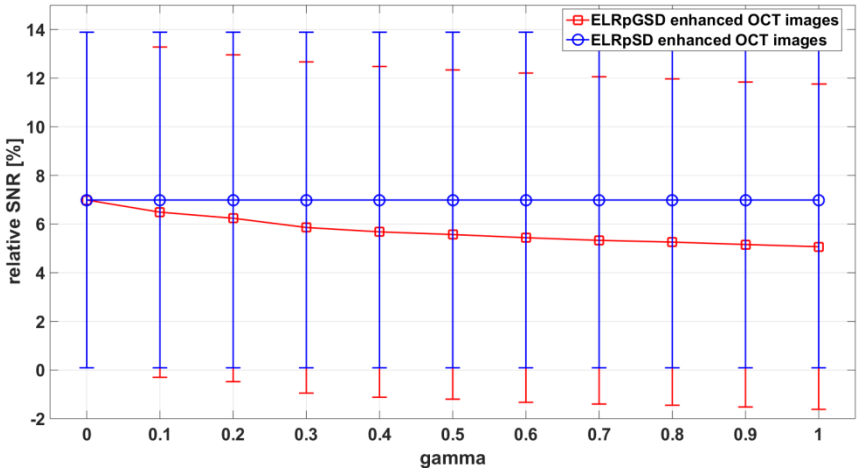

Figure 6. Average of relative SNR values (in percentage) estimated from 10 3D OCT images enhanced with: circles - the ELRpSD method; squares - the ELRpGSD method as a function of regularization constant γ, see Eq.(6) and (13).

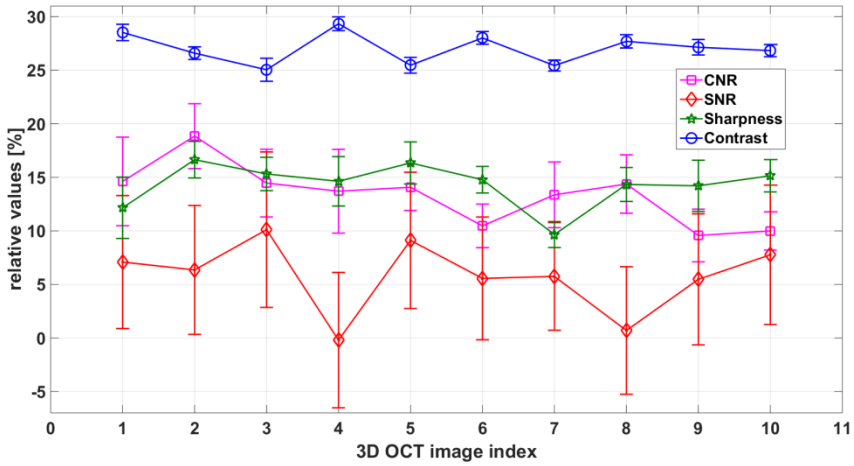

Figure 7. Relative values of image quality metrics for each of 10 3D OCT images enhanced with the ELRpGSD algorithm with γ=0.4. Squares: CNR; stars: sharpness; circles: contrast; diamonds: SNR.

4 DISCUSSION

Speckle stands for major obstacle in quantitative OCT image analysis. Due to its dual role as a source of noise and as a carrier of information about tissue microstructure its complete reduction is not desirable. Thus, it is a challenge to increase the CNR value, which is used as a figure of merit in speckle reduction, and preserve image resolution, contrast and fidelity of edges. We have proposed approach to speckle reduction which is based on decomposition of 2D OCT scans into low-rank approximation of the "clean" image and group sparse term which takes into account speckle. In comparison with our previous contribution [14], the new algorithm relies on group sparsity based regularization instead of sparsity only. Group sparisty constraint enforces more speckle from the noise related group to be absorbed by the sparse matrix in additive low-rank plus sparse decomposition of 2D OCT image. Hence, proposed method yields better low-rank approximation of the original OCT images with simultaneously increased values of CNR, sharpness, contrast and SNR. Moreover, increase of the value of CNR and contrast can be controlled by the value of group sparsity regularization constant. Thus, depending on the relative importance of the each image quality metric the group sparsity regularization can bring additional improvement of the quality of OCT images.

5 CONCLUSIONS

We have developed a method for additive low-rank and sparse matrix decomposition and applied it for the speckle reduction in OCT images. In comparison with state-of-the-art low-rank and sparse decomposition methods proposed method uses more accurate measure of rank and group sparsity constraint implemented through combination of ℓ_1- and ℓ_2-norm of the sparse term in additive decomposition. Thus, the method is named the ELRpGSD algorithm. The method, which is applied on individual 2D OCT scans, was tested on 10 3D OCT images comprised of 64 scans each. It was able to simultaneously increase, relative to the original OCT images, values of CNR, contrast and

sharpness (improved fidelity of edges) and SNR. Furthermore, by the regularization constant associated with the ℓ_2-norm of the sparse term values of CNR and contrast of enhanced image can be increased relatively to the values of original images.

ACKNOWLEDGEMENTS

This work was supported in parts through: Croatian Science Foundation Grant IP-2016-06-5235; Bilateral Chinese-Croatian Grant "Structure constrained decompositions for enhancement and segmentation of PET/CT and OCT images"; the European Regional Development Fund under the grant KK.01.1.1.01.0009 (DATACROSS); the National Basic Research Program of China (973 Program) under Grant No. 2014CB748600; the National Natural Science Foundation of China (NSFC) under Grant No. 61622114.

REFERENCES

[1] Soest, van G., Villiger, M., Regar, E., Tearney, G. J., Bouma, B. E., Steen, van der A. F., "Frequency domain multiplexing for speckle reduction in optical coherence tomography," J. Biomed. Opt. 17. 076018 (2012).

[2] Schmitt, J. M., Xiang, S. H., Yung, K. M., "Speckle in optical coherence tomography: an overview," J. Biomed. Opt. 4, 95-105 (1999).

[3] Goodman, J. W., "Statistical properties of laser speckle patterns," in: Dainty, J. C. (Ed.), [Laser speckle and related phenomena], Springer Verlag (1984).

[4] Karamata, B., Hassler, K., Laubscher, M., Lasser, T., "Speckle statistics in optical coherence tomography," J. Opt. Soc. Am. A. 22, 593-596 (2005).

[5] Zhang, X., Li, L., Zhu, F., Hou, W W., Chen, X., "Spiking cortical model-based nonlocal means method for speckle reduction in optical coherence tomography images," J. Biomed. Opt. 19, 066005 (2014).

[6] Cheong, W. F., Prahl, S. A., Welch, A. J., "A review of the optical properties of biological tissues," IEEE J. Quant. Electr. 26, 2166-2185 (1990).

[7] Wilson, B. C., Jacques, S. L., "Optical reflectance and transmittance of tissues-principles and applications," IEEE J. Quant. Electr. 26, 2186-2199 (1990).

[8] Wilkins, G. R., Houghton, O. M., Oldenburg, A. L., "Automated segmentation of intraretinal cystoid fluid in optical coherence tomography," IEEE Trans. Biomed. Eng. 59, 1109-1114 (2012).

[9] Chen, H., Chen, X., Qiu, Z., Xiang, D., Chen, W., Shi, F., Zheng, J., Zhu, W., Sonka, M., "Quantitative analysis of retinal layers' optical intensities on 3D optical coherence tomography for central retinal artery occlusion," Scientific Reports 5, 9269 (2015).

[10] Xu, C., Schmitt, J. M., Carlier, S. G., Virmani, R., "Characterization of atherosclerosis plaques by measuring both backscattering and attenuation coefficients in optical coherence tomography," J. Biomed. Opt. 13, 034003 (2008).

[11] Marks, D. L., Ralston, T. S., Boppart, S. A., "Speckle reduction by I-divergence regularization in optical coherence tomography," J. Opt. Soc. Am. A. 22, 2366-2371 (2005).

[12] Ozcan, A., Bilenca, A., Desjardins, A. E., Bouma, B. E., Tearney, G. J., "Speckle reduction in optical coherence tomography images using digital filtering," J. Opt. Soc. Am. A. 24, 1901-1910 (2007).

[13] Adler, D. C., Ko, T. H., Fujimoto, J. G., "Speckle reduction in optical coherence tomography images by use of a spatially adaptive wavelet filter," Opt. Lett. 29, 2878-2880 (2004).

[14] Kopriva, I., Shi, F., Chen, X., "Enhanced low-rank + sparsity decomposition for speckle reduction in optical coherence tomography," J. Biomed. Opt. 21, 076008 (2016).

[15] Huang, H. H., Liu, X. Y., Liang, Y., "Feature Selection and Cancer Classification via Sparse Logistic Regression with the Hybrid $L_{1/2+2}$ Regularization," PLoS One, e0149675 (2016).
[16] Tibshirani, R., Saunders, M., Rosset, S., Zhu, J., Knight, K., "Sparsity and smoothness via fused lasso," J. Roy. Stat. Soc. B 67, 91-108 (2005).
[17] Candès, E. J., Li, X., Ma, Y., Wright, J., "Robust principal component analysis?," J. ACM 58, 11 (2011).
[18] Chandrasekaran, V., Sanghavi, S., Parillo, P. A., Willsky, A. S., "Rank-sparsity incoherence for matrix decomposition," SIAM J. Opt. 21, 572-596 (2011).
[19] Zhou, T., Tao, D., "GoDec: Randomized Low-rank & Sparse Matrix Decomposition in Noisy Case," in Proc. 28th Int. Conf. Machine Learning (2011), pp. 33-40.
[20] Chartrand, R., "Nonconvex Splitting for Regularized Low-Rank + Sparse Decomposition," IEEE Trans. Sig Proc. 60, 5810-5819 (2012).
[21] Recht, B., Fazel, M., Parillo, P. A., "Guaranteed minimum-rank solutions of linear matrix equations via nuclear norm minimization," SIAM Rev. 52, 471-501 (2010).
[22] Tropp, J., A., Gilbert, A. C., "Signal Recovery from Random Measurements via Orthogonal Matching Pursuit," IEEE Trans. Inf. Theory 53, 4655-4666 (2007).
[23] Kim, S., J., Koh, K., Lustig, M., Boyd, S., Gorinevsky, D., "An Interior-Point Method for Large-Scale -Regularized Least Squares," IEEE J. Sel. Top. Sig. Proc. 1, 606-617 (2007).
[24] Zhang, X., Xu, C., Sun, X., Baciu, G., "Schatten-q regularizer for low rank subspace clustering model," *Neurocomputing* 182, 36-47 (2016).
[25] Mohan, K., Fazel, M., "Iterative reweighted algorithms for matrix rank minimization," J. Mach. Learn. Res. 13, 3441-3473 (2012).
[26] Parekh, A., Selesnick, I. W., "Enhanced Low-Rank Matrix Approximation," IEEE Sig. Proc. Lett. **23**, 493-497 (2016).
[27] Lu, C., Tang, J., Yan, S., Lin, Z., "Generalized nonconvex nonsmooth low-rank minimization," in Proceedings of the IEEE Conference on Computer Vision and Pattern Recognition (IEEE 2014), pp. 4130-4137.
[28] Lu, C., Zhu., C., Xu, C., Yan, S., Lin, Z., "Generalized singular value thresholding," in Twenty-Ninth AAAI Conference on Artificial (AAAI 2015), pp. 1805-1811.
[29] Chen, P., Y., Selesnick, I., "Group-Sparse Signal Denoising: Non-Convex Regularization, Convex Optimization," IEEE Trans. Sig. Proc. 62, 3464-3476 (2014).
[30] Zou, H., Hastie, T., "Regularization and variable selection via the elastic net," J. Roy. Stat. Soc. B 67, 301-320 (2005).
[31] Yu, Y., "On decomposing the proximal map," in Proceedings of the 26th International Conference on Neural Information Processing Systems (NIPS 2013), pp. 91-99 .
[32] Baghaie, A., 'Souza, R. M., Yu, Z., "Sparse and Low Rank Decomposition Based Batch Image Alignment for Speckle Reduction of Retinal OCT Image," in Proceedings of the 2015 IEEE International Symposium on Biomedical Imaging (IEEE 2015), pp. 226-230.
[33] Luan, F., Wu, Y., "Application of RPCA in optical coherence tomography for speckle noise reduction," Laser Phys. Lett. 10, 035603 (2013).
[34] Donoho, D. L., Elad, M., "Optimally sparse representation in general (non-orthogonal) dictionaries via *l*1 minimization," Proc. Nat. Acad. Sci. 100, 2197-2202 (2003).
[35] Donoho, D., "De-noising by soft-thresholding," IEEE Trans. Inf. Theory 41, 613-627 (1995).
[36] Pustelnik, N., Condat, L., "Proximity Operator of a Sum of Functions; Application to Depth Map Estimation," IEEE Sig. Proc. Lett. 24, 1827-1831 (2017).
[37] Boyd, S., Parikh, N., Chu, E., Peleato, B., Eckstein, J., "Distributed optimization and statistical learning via the alternating direction method of multipliers," Found. Trends Mach. Learn. 3, 1-122 (2010).
[38] Bertsekas, D. P., [Constrained Optimization and Lagrange Multiplier Methods], Athena Scientific (1996).

[39] Panetta, K., Gao, C., Agaian, S., “No reference color image contrast and quality measure, ” IEEE Trans. Cons. Elec. 59, 643-651 (2013).
[40] Oh, T. H., Tai, Y. W., Bazin, J. C., Kim, H., Kweon, I. S., "Partial sum minimization of singular values in robust PCA: algorithms and applications," IEEE Trans. Patt. Anal. Mach. Int. 38, 744-758 (2016)
[41] MATLAB code for 2D bilateral filtering algorithm. http://www.mathworks.com/matlabcentral/fileexchange/12191-bilateral-filtering
[42] Chen, H, Chen, X., Qiu, Z., Xiang, D., Chen, W., Shi, F., Zheng, J., Zhu, W, M. Sonka, M., "Quantitative analysis of retinal layers' optical intensities on 3D optical coherence tomography", Investigative Ophthalmology & Visual Science 54, 6846-6851 (2013).